



## Original Articles

# Inositol hexaphosphate enhances chemotherapy by reversing senescence induced by persistently activated PERK and diphthamide modification of eEF2



Binghui Xu <sup>a,b,1</sup>, Qingan Jia <sup>a,b,1</sup>, Xia Liao <sup>c</sup>, Tian Fan <sup>a</sup>, Lei Mou <sup>a</sup>, Yuna Song <sup>a</sup>, Chunyu Zhu <sup>a</sup>, Tongling Yang <sup>a,b</sup>, Zhixian Li <sup>a</sup>, Miao Wang <sup>a</sup>, Qiangbo Zhang <sup>d,\*,\*\*</sup>, Lei Liang <sup>e,\*</sup>

<sup>a</sup> Xi'an Key Laboratory of Stem Cell and Regenerative Medicine, Institute of Medical Research, Northwestern Polytechnical University, Xi'an 710038, China

<sup>b</sup> Shaanxi Provincial Key Laboratory of Infection and Immune Disease, Shaanxi Provincial People's Hospital, Xi'an 710038, China

<sup>c</sup> Department of Nutrition, First Affiliated Hospital of Xi'an JiaoTong University, Xi'an 710038, China

<sup>d</sup> Department of General Surgery, Qilu Hospital, Shandong University, Jinan 250012, China

<sup>e</sup> Department of Oncology, Shanghai Medical College, Fudan University, Shanghai 200032, China

## ARTICLE INFO

**Keywords:**

Colorectal cancer  
Endoplasmic reticulum stress  
Senescence  
Chemoresistance

## ABSTRACT

Oxaliplatin is an important initial chemotherapy benefiting advanced-stage colorectal cancer patients. Frustratingly, acquired oxaliplatin resistance always occurs after sequential chemotherapy with diverse antineoplastic drugs. Therefore, an exploration of the mechanism of oxaliplatin resistance formation in-depth is urgently needed. We generated oxaliplatin-resistant colorectal cancer models by four representative compounds, and RNA-seq revealed that oxaliplatin resistance was mainly the result of cells' response to stimulus. Moreover, we proved persistent stimulus-induced endoplasmic reticulum stress (ERs) and associated cellular senescence were the core causes of oxaliplatin resistance. In addition, we screened diverse phytochemicals for ER inhibitors *in silico*, identifying inositol hexaphosphate (IP6), whose strong binding was confirmed by surface plasmon resonance. Finally, we confirmed the ability of IP6 to reverse colorectal cancer chemoresistance and investigated the mechanism of IP6 in the inhibition of diphthamide modification of eukaryotic elongation factor 2 (eEF2) and PERK activation. Our study demonstrated that oxaliplatin resistance contributed to cell senescence induced by persistently activated PERK and diphthamide modification of eEF2 levels, which were specifically reversed by combination therapy with IP6.

## 1. Introduction

Colorectal cancer (CRC) is the third most frequent cancer worldwide and ranks second in mortality; its malignant progression is multifaceted [1]. Much clinical progress has been made, including surgical resection, cytotoxic chemotherapy, molecular-targeted therapy, immunotherapy, and combination treatment strategies. More than 50 % of CRC patients fail treatment, and their general prognosis remains dismal [2]. Oxaliplatin-based chemotherapy is a key component of first-line treatment for CRC patients with advanced-stage disease or metastatic lesions; however, its clinical efficacy is unsatisfactory because of acquired chemoresistance [3]. Therefore, improved efficacy of chemotherapies is

urgently needed [4].

Endoplasmic reticulum (ER) stress is a primary contributor to chemoresistance, acting as a tumor surveillance mechanism [5]. The ER is an intracellular organelle required for newly synthesized protein folding and assembly [6]. Under physiological conditions, glucose-regulating protein 78 (GRP78) binds to and inhibits the activity of stress sensors that serve as ER stress regulators, including inositol-requiring enzyme 1 $\alpha$  (IRE1 $\alpha$ ), activating transcription factor 6 (ATF6), and protein kinase R-like ER kinase (PERK). Traditional cytotoxic chemotherapies cause cell cycle withdrawal but often fail to fully wipe out the tumor burden due to the development of chemoresistance [7]. Recent studies have found that persistent ER stress is a major defensive mechanism forcing

\* Corresponding author.

\*\* Corresponding author.

E-mail addresses: [zqb-sd@163.com](mailto:zqb-sd@163.com) (Q. Zhang), [llknight115@163.com](mailto:llknight115@163.com) (L. Liang).

<sup>1</sup> These authors contributed equally to this work.

cell evolution [8]. The collapse of the unfolded protein response (UPR) directly contributes to cell death or the reversion of chemoresistance [9]. Because cellular ER stress is often regarded as an anticancer mechanism, exploring the regulation of UPR signaling and its implications could open new therapeutic avenues in reversing tumor chemoresistance [10].

The UPR determines cell fate related to ER quality control pathways governing transcriptional reprogramming and messenger RNA (mRNA) decay, global translational attenuation, and removal of misfolded proteins to ensure the fidelity of ER protein [11]. Eukaryotic translation elongation factor 2 (eEF-2) is an essential mediator of protein synthesis that catalyzes ribosomal translocation. During ER stress, reduced global protein synthesis is key to restoring tumor cell homeostasis. Otherwise, the tumor cells will die [12]. Inactivation of eEF-2 reduces protein synthesis; this inactivation is regulated by several post-translational mechanisms, such as adenosine diphosphate-ribosylation (ADPr) and phosphorylation [13]. Phosphorylated PERK (*P*-PERK) can also reduce the protein load in response to ER stress using translation initiation factor2- $\alpha$  (eIF2 $\alpha$ ) as a downstream effector [14]. Because decreased protein synthesis is a key mechanism for restoring tumor cell homeostasis during ER stress, we speculated that chemoresistance could be reversed by blocking UPR. Recently, phytochemicals have been reported to have anticancer effects alone or combined with chemotherapeutic drugs; however, the specific targets and related mechanisms remain unclear [15,16].

In this study, we generated oxaliplatin-resistant colorectal cancer models by four representative compounds and found that oxaliplatin resistance was mainly the result of the cell's response to stimulus. In addition, we proved persistent stimulus-induced ER stress and associated cellular senescence were the core causes of oxaliplatin resistance. Moreover, we evaluated the affinity between antioxidative phytochemicals and ER stress sensors by screening the Database of US Food and Drug Administration-approved drugs in silico and confirmed inositol hexaphosphate (IP6) had the lowest binding energy with diphthamide biosynthesis gene 1 (DPH1) and GRP78 by surface plasmon resonance (SPR). Finally, we confirmed the ability of IP6 to reverse colorectal cancer chemoresistance, and investigated the mechanism of IP6 in inhibition of diphthamide modification of eukaryotic elongation factor 2 (eEF2) and PERK activation. Our study demonstrated that oxaliplatin resistance contributed to cell senescence induced by persistently activated PERK and diphthamide modification of eEF2 levels, which were specifically reversed by combination therapy with IP6.

## 2. Materials and methods

### 2.1. Cell lines and cell culture

HCT-15 and HT-29 cells were obtained from the Cell Bank of Type Culture Collection of the Chinese Academy of Sciences (Shanghai, China). HCT-15 cells were cultured in RPMI1640 medium (Gibco), and HT29 cells were cultured in McCoy's 5 A medium (Gibco). All media were supplemented with 10 % fetal bovine serum. All cells were maintained in 5 % CO<sub>2</sub> at 37 °C.

### 2.2. Clinical specimens, mouse tumor tissues, and immunohistochemistry

Surgically removed tumor tissues from 203 patients were used to investigate the role of phosphorylated PERK in clinicopathology. All tumor tissue was obtained from the Department of Colorectal Surgery of the Fudan University Shanghai Cancer Center, and the histopathologic diagnosis was confirmed by pathologists. Written consent and ethical approval were obtained from the Research Ethics Committee of Fudan University (Permit Number: 2020-058). Subcutaneous and abdominal HCT-15 tumors from BALB/c nu mice were used to examine ER stress and chemoresistant protein expression. Immunohistochemistry was performed as previously described [17]. Briefly, tumor tissue was fixed

and paraffin-embedded. Tumor sections (5-μm thick) were stained for *Anti*-ABCC1 (1:100, R&D #MAB19291); *Anti*-GRP78 (1:100, HUABIO #ER1706-50); *Anti*-pPERK (1:200, Affinity Biosciences #DF7576); *Anti*-HIF1 $\alpha$  (1:200, Affinity Biosciences #BF8002).

### 2.3. Generation of ER stress CRC cell models

CRC cell lines HCT-15 and HT-29 were treated with an initial concentration of 0.5 μM oxaliplatin for 7 days. After passage, the cells were incrementally treated with higher oxaliplatin concentrations (1, 2, and 4 μM) from day 10 to day 30. After 30 days, the cells were maintained in 4 μM oxaliplatin. The stably resistant cells were named HCT-15-Oxa and HT-29-Oxa. Similarly, HCT-15 and HT-29 were treated with sorafenib to generate the sorafenib-resistant cell lines HCT-15-Sora and HT-29-Sora. HCT-15 and HT-29 were treated with a single concentration of oxaliplatin (2 μM) or sorafenib (1 μM) for more than 30 days, resulting in cell lines HCT-15-Oxa(s), HT-29-Oxa(s), HCT-15-Sora(s), and HT-29-Sora (s). CoCl<sub>2</sub>, brefeldin A, or low glucose-resistant CRC cells were generated by growing cells in increasing concentrations of the agents until the cells became tolerant. The resulting cell lines were HCT-15-CoCl<sub>2</sub>, HCT-15-Bre, and HCT-15-Lowg, respectively.

### 2.4. RNA sequencing (RNA-seq) and data analysis

Total RNA was extracted from CRC cells using TRIzol Reagent (Invitrogen, Thermo Fisher Scientific, Waltham, MA, USA), and mRNA was extracted and sheared into 200-base fragments. The fragmented mRNA was reverse-transcribed into complementary DNA (cDNA), which was amplified by PCR to generate the cDNA library. The cDNA library was sequenced using the Illumina NovaSeq 6000 platform. Differentially expressed genes (DEGs) were identified with the DESeq software package using the following criteria: Q (adjusted p-value) < 0.05; fold-change ≥2. Gene Ontology (GO) and Kyoto Encyclopedia of Genes and Genomes (KEGG) enrichment analyses were performed on the identified DEGs. The GO terms and KEGG pathways with p < 0.05 were considered significantly enriched among the DEGs. All data were uploaded to the Gene Expression Omnibus (GSE227641).

### 2.5. Lentiviral infection

The biosynthesis of diphthamide has been proposed to involve a multi-step pathway that includes seven diphthamide biosynthesis proteins (DPH1–DPH7) in humans, with DPH1 required for the first step in the synthesis of diphthamide as a rate-limiting enzyme [18]. Complementary oligonucleotides targeting DPH1 and scramble control were annealed and cloned into PLKO.1. The shDPH1 targeting sequence was 5'-GCTTACCGGTATGACCCATAT-3'. The Flag-DPH1 and hemagglutinin-eEF-2 lentiviral overexpression vectors (pCDH-CMV-MCS-EF1-Puro) were from Rosetta Stone Biotech Co. (China). Lentiviruses were produced in CRC cells co-transfected with lentiviral expression and packaging vectors. The viral supernatant was collected 48 h after transfection. CRC cells were infected with lentivirus in the presence of 8 μg/mL polybrene for 48 h and selected with puromycin (2 μg/mL) for a week.

### 2.6. Construction of the eEF2<sup>G717R</sup> plasmid

To construct an eEF2 point mutant plasmid, the wild-type eEF2-pCMV-tag2B plasmid was used as the PCR template, and the PCR-amplified product was treated with the methylase *Dpn*I. The eEF2 mutant plasmid was then validated by sequencing. The primers designed were as follows: eEF2<sup>G717R</sup> Forward, 5'-ctggcccccctctcggtggatgg-3'; and eEF2<sup>G717R</sup> Reverse, 5'-ccatccaccgcagagggccag-3'. The cells were transfected with the recombinant plasmid using Lipofectamine 3000 (Invitrogen) following the manufacturer's instructions.

## 2.7. ADPr assay

Cells were lysed on ice in radioimmunoprecipitation assay buffer containing a protease inhibitor cocktail (Roche, 11,697,498,001). Total cell extracts (50 µg) were incubated for 60 min at 25 °C in ADPr buffer [20 mM Tris-HCl (pH 7.4), 1 mM EDTA, and 5 mM MgCl<sub>2</sub>] containing 25 µM biotinylated nicotinamide adenine dinucleotide (R&D Systems, 670-500-01) and 500 µg/L diphtheria toxin (Sigma-Aldrich, D0564). Proteins were separated by sodium dodecylsulfate-polyacrylamide gel electrophoresis and transferred to polyvinylidene fluoride membranes. The membranes were incubated with HRP-conjugated streptavidin to detect the biotin-ADPr-eEF2.

## 2.8. SA-β-gal staining

CRC cells were seeded into six-well plates at a cell density of 0%–50%. After cell attachment, the medium was removed, and the cells were washed once with phosphate-buffered saline. SA-β-gal staining was performed using the SA-β-gal staining kit (Beyotime, China), according to the manufacturer's instructions. Briefly, SA-β-gal (1 mL) was added to each well, and the cells were incubated overnight at 37 °C. Cells binding β-gal turned blue. Six randomly selected fields were observed using an optical microscope.

## 2.9. Co-immunoprecipitation and immunoblotting

Cells endogenously or exogenously expressing the proteins of interest were lysed in IP (immunoprecipitation) lysis buffer (Pierce, 87,787) supplemented with a protease inhibitor cocktail (Roche, 11,697,498,001). For endogenous co-immunoprecipitation, cell lysates were incubated with specific antibodies at 4 °C overnight and then incubated with protein A/G Sepharose for 2 h. Cell lysates directly incubated with Sepharose beads conjugated with mouse/rabbit IgG served as a negative control. For exogenous co-immunoprecipitation, cell lysates were incubated with anti-Flag/hemagglutinin resin beads at 4 °C overnight. The beads were washed four times with cold Tris-buffered saline-Tween20 buffer, and the immunoprecipitates were enriched and denatured at 99 °C for 5 min in 2 × loading buffer.

## 2.10. Molecular docking and real-time SPR analysis

Molecular docking is a structure-based computational algorithm for compound screening. Molecular docking was performed using the PyRx virtual screening tool AutoDock Vina to identify the binding mode of the desired protein with select phytochemicals [19].

Real-time SPR analysis was performed on a Biacore ×100 apparatus (GE Healthcare) at 25 °C in HBS-EP + buffer (10 mM HEPES, 150 mM NaCl, 3 mM EDTA, 0.05 % Tween20). GRP78 and DPH1 (200 µg/mL) in 10 mM acetate pH 4.5 were covalently immobilized on a CM5S sensor chip (GE Healthcare) at 2176 resonance units using the amine coupling protocol provided by the manufacturer. The IP6 kinetic titration experiments (single-cycle kinetics) were performed at a 30 µL/min flow rate with two-fold serial dilutions (0–700 µM). All curves were evaluated using ×100 Evaluation Software 3.0 (GE Healthcare) after double-referencing subtraction with a bivalent fitting model.

## 2.11. Transmission electron microscopy

Transmission electron microscopy was performed as previously described [20]. Briefly, cells were harvested, pelleted, and fixed in 2.5 % glutaraldehyde in cacodylate buffer. After rinsing with cacodylate buffer, the cells were fixed with 1 % OsO<sub>4</sub> for 6 h. After dehydration with graded alcohols, the samples were embedded in epoxy resin. Ultrathin sections were obtained and stained with uranyl acetate and lead citrate. Sections were photographed using a Jeol 1200 EX 11 transmission electron microscope.

## 2.12. TCGA dataset analysis using GEPIA2 and STRING

The correlations between ABCC1 expression and four signatures in colon and rectal adenocarcinoma defined with GRP78, ATF6, PERK, and IRE1α were analyzed using GEPIA2 [21]. The online tool STRING was used to predict the function of genes and gene sets, including protein and genetic interactions, pathways, co-expression, co-localization, and protein domain similarity among the genes related to ER stress, senescence, and chemoresistance. The prediction output graphically presented the network that depicts the relationships between the genes and gene sets associated with these processes [22].

## 2.13. In vivo evaluation of tumor proliferation and metastasis

HCT-15 cells ( $5 \times 10^6$  cells in phosphate-buffered saline; 0.1 mL) were injected into the right sides of the necks of 4-week-old male BALB/c nu mice (n = 6/group). Mice were treated orally with IP6 (2 mg/kg/d) with or without an intraperitoneal injection of oxaliplatin (10 mg/kg/w). After 5 weeks, subcutaneous tumor-bearing mice were euthanized, and the tumor volumes were evaluated. For the peritoneal metastatic tumor model, HCT-15-luciferase CRC cells were injected intraperitoneally. Mice were examined for luciferase activity using D-luciferin (100 mg/kg; Invitrogen, Life Technologies). Images were captured using the PerkinElmer IVIS Lumina III instrument. Image analysis was performed with Living Image Software (IVIS Lumina Series software). The overall survival (OS) time was also evaluated. To evaluate the synergistic antitumor effect of oxaliplatin combined with an intraperitoneal injection of PERK activator (1 mg/kg/d) or PERK inhibitor, subcutaneous xenograft models were established using HCT-15 cells ( $5 \times 10^6$  cells). Mice were treated with an intraperitoneal injection of oxaliplatin (10 mg/kg/w). After 4 weeks, subcutaneous tumor-bearing mice were euthanized, and the tumor weights were evaluated. Tumor growth was significantly inhibited by treatment with the PERK activator CCT020312, (p = 0.0012). When combined with oxaliplatin, the tumor weights did not decrease further (p > 0.05). Conversely, when treated with the PERK inhibitor GSK2656157, the tumor weights increased (p = 0.0019), and a significant synergistic antitumor effect occurred when combined with oxaliplatin treatment.

Mice were euthanized at the end of the study with an intraperitoneal injection of 5 mg/kg pentobarbital followed by cervical dislocation. The study protocol was approved by the Institutional Animal Care and Use Committee of Northwestern Polytechnical University, and all methods were performed in accordance with the relevant guidelines.

## 2.14. Statistical analysis

Statistical analysis was performed using GraphPad Prism 7.0 software (GraphPad Software, Inc.). The complete response rates and OS times between patients in different groups were compared with Kaplan-Meier analysis using the Cox–Mantel log-rank test. Quantitative differences in tumor volumes, gene, and protein expression levels, and cell numbers were evaluated by the Student's t-test. Multiple groups were compared using a one-way analysis of variance with the post-hoc Tukey's multiple comparison test. Data are presented as the mean ± standard deviation (n = 3 independent experiments). p < 0.05 was considered to be significant.

## 3. Results

### 3.1. CRC treated by four representative compounds exhibited oxaliplatin resistance with the mechanism of response to stimulus

Systemic oxaliplatin-based chemotherapy, such as FOLFOX (leucovorin, fluorouracil, and oxaliplatin), is commonly used for advanced-stage CRC patients, with initial chemotherapy benefiting, but resistance is often acquired [23]. Based on four common reactions to

chemotherapy, we generated four oxaliplatin-resistant CRC cell lines (HCT-15-Oxa, HCT-15-Sora, HCT-15-CoCl<sub>2</sub>, and HCT-15-Lowg, Fig. S1) under the conditions of oxaliplatin, sorafenib, CoCl<sub>2</sub>, and low glucose. All of the above CRC cell lines exhibited increased oxaliplatin IC<sub>50</sub> values.

RNA-Seq identified DEGs in four oxaliplatin-resistant CRC cell lines (Fig. 1A–D), and DEGs from HCT-15-Oxa, HCT-15-Sora, and HCT-15-Lowg had multiple gene overlap (Fig. 1E). GO enrichment analysis for overlapping DEGs showed the enrichment in response to stimulus (Fig. 1F and G). Based on The Cancer Genome Atlas (TCGA) database, we analyzed the relationships between individual MRP subfamily genes and ER stress genes and identified positive correlations between MRP gene signatures (ABCC1–5) and ER stress gene signatures (GRP78, PERK, ATF6, and IRE1) in colon and rectal adenocarcinoma ( $R = 0.37$ ). In particular, there were positive correlations between PERK and ABCC1 ( $R = 0.41$ ) and ABCA1 ( $R = 0.47$  Fig. 1H and I). Furthermore, immunohistochemistry on tumor tissues from CRC patients who underwent oxaliplatin-based neoadjuvant chemotherapy confirmed the upregulated expression of HIF1 $\alpha$ , ABCC1, and PERK (Fig. S2).

We next used a subcutaneous HCT-15 mouse tumor model to evaluate the effects of oxaliplatin on CRC (Fig. 1J and K). Treatment with oxaliplatin reduced tumor volume compared to that of the control group; however, oxaliplatin could not completely eliminate the tumors, and there were increased levels of HIF1 $\alpha$ , ABCC1, PERK, and P-PERK in the residual tumors (Fig. 1L). TEM also revealed the dilated, cystic ER structures in the oxaliplatin-treated tumor tissues (Fig. 1M). Together, these findings demonstrated that CRC enhanced oxaliplatin resistance was the result of response to stimulus, exhibiting activated ER stress.

### 3.2. Persistent external stimulus enhanced oxaliplatin resistance in CRC cells, whereas the resistance phenotype caused by short-term stimulus varied

Most cancers are often sensitive to initial chemotherapy; however, resistance always occurs after long-term chemotherapy and is accompanied by ER stress activation and UPR [10]. Therefore, we explored the differences between short-term and long-term sequential stimulus-induced ER stress and their effects on chemosensitivity in CRC.

A 3-day short-term stimulus of HCT-15 cells with CoCl<sub>2</sub>, brefeldin A, low glucose, oxaliplatin, or sorafenib increased the number of stress granules (as determined by TIAR and G3BP1-positive staining) in the CRC cells compared to those observed in the wild-type cells. Sequential stimulus of HCT-15 cells with these five compounds for more than 30 days also resulted in significantly higher TIAR and G3BP1 levels than the control cells, whereas the levels of stress granules under short-term and sequential stimuli varied (Fig. 2A). In addition, we treated HCT-15 and HT-29 CRC cells within increasing concentrations of oxaliplatin, which resulted in a transformed phenotype with reduced intercellular adhesion, reshaped the cell morphologies with longer tentacles, and increased granule deposition in the cytoplasm (Fig. S3A). The numbers of stress granules and ER-related biomarkers were also significantly upregulated in HT-29-OXA cells (Fig. S4). During the incremental stimulus with increasing oxaliplatin concentrations, HCT-15 and HT-29 gradually acquired oxaliplatin resistance with corresponding increases in P-PERK and ABCC1 levels (Fig. 2B, Fig. S3B). After more than 30 days of oxaliplatin treatment, oxaliplatin resistance became stable, and the cell lines were named HCT-15-Oxa ( $p < 0.001$ ; Fig. 2B) and HT-29-Oxa ( $p = 0.004$ ; Fig. S3B), with significantly increased IC<sub>50</sub>s and upregulated P-PERK and ABCC1 levels compared to those of the wild-type cells.

We also treated the CRC cells sequentially with increasing concentrations of sorafenib (Fig. 2C). After treating with sorafenib for no more than 10 days, the CRC cells exhibited decreased resistance to oxaliplatin (i.e., lower oxaliplatin IC<sub>50</sub>s) and decreased ABCC1 levels but increased P-PERK levels (Fig. 2C, Fig. S3C). Interestingly, when sorafenib treatment continued for more than 21 days, oxaliplatin resistance gradually increased. Persistent sorafenib treatment over 30 days resulted in the

sorafenib-resistant CRC cell lines HCT-15-Sora and HT-29-Sora. These cell lines exhibited significantly enhanced resistance to oxaliplatin with higher IC<sub>50</sub>s and increased P-PERK and ABCC1 levels compared to the wild-type cells (Fig. 2C and Fig. S3C).

We also treated CRC cells with CoCl<sub>2</sub>, brefeldin A, or low glucose, common inducers of ER stress related to hypoxia simulation, nutrient deprivation, and blocking of protein transporters. When treated with CoCl<sub>2</sub> for 3 days or more than 30 days, both HCT-15 (Fig. 2D) and HT-29 (Fig. S3D) exhibited increased oxaliplatin resistance (i.e., higher IC<sub>50</sub>s). Short-term and sequential treatments with low glucose also enhanced oxaliplatin resistance, and HCT-15-Lowg and HT-29-Lowg cells were more resistant to oxaliplatin than short-term cultures (Fig. 2E and Fig. S3E). Brefeldin A is a classic ER stress inducer [24]. After short-term treatment with brefeldin A, oxaliplatin resistance decreased. In contrast, treatment for more than 30 days resulted in significant oxaliplatin resistance in HCT-15-Bre and HT-29-Bre cells and higher P-PERK and ABCC1 expression levels (Fig. 2F, Fig. S3F).

Together, these findings demonstrated that persistent external stimulus enhanced oxaliplatin resistance in CRC cells, whereas the resistance phenotype caused by short-term stimulus varied.

### 3.3. Oxaliplatin-resistant CRC cells resulting from long-term stimulus with diverse compounds induced senescence

Sorafenib has multiple molecular targets and exhibits the same resistance to oxaliplatin after long-term sequential treatment in CRC [25]. In this study, the upregulation of senescence-associated genes (e.g., FN1, ATM, CDKN1A, and RB1) was confirmed by PCR array (Fig. 3A). Furthermore, senescence-associated  $\beta$ -galactosidase (SA- $\beta$ -gal) staining showed an increased number of senescent cells in the HCT-15-Oxa culture after long-term oxaliplatin treatment (Fig. 3B). Immunoblotting also confirmed higher levels of senescence-related proteins, including H2AX, Ki67, and IL-6 in HCT-15-Oxa (Fig. 3C). Similarly, PCR array and immunoblotting confirmed the upregulation of senescence-associated genes and proteins (Fig. 3D, F). SA- $\beta$ -gal staining also revealed an increased number of senescent cells after long-term sorafenib treatment (Fig. 3E). Moreover, CRC cells treated with CoCl<sub>2</sub>, brefeldin A, or low glucose for more than 30 days exhibited an increased number of senescent cells (Fig. 3G). Immunoblotting confirmed increased levels of senescence-associated proteins (Fig. 3H). Together, these findings showed that continuous stimulus with diverse compounds enhanced oxaliplatin resistance and increased the proportion of senescent cells.

### 3.4. PERK acted as a key regulator of malignant CRC progression relating senescence and translational elongation inhibition

Because we established that ER stress, senescence, and oxaliplatin resistance were closely correlated, we searched for the core molecules that could regulate all three processes. Using STRING, we evaluated the key proteins involved in ER stress, senescence, and chemoresistance. We found that the ER sensors PERK/EIF2AK3 played a central role in these processes (Fig. 4A). Using LinkedOmics, we found that PERK was negatively related to translational elongation (Fig. 4B). We also analyzed the correlations between senescence signatures (ten senescence-associated genes) and PERK using GEPIA2. We observed the most positive correlation between PERK and the senescence signatures ( $R = 0.42$ , Fig. 4C).

It has been reported that PERK induces cell cycle arrest in G1, which may regulate cancer cell dormancy [26]. Based on our findings, we focused on P-PERK and explored its clinicopathological roles in CRC. A cohort of 203 patients was dichotomized according to high and low P-PERK levels (Fig. 4D). High P-PERK levels were detected in 73 out of the 203 CRCs (35.96 %), and low expression of P-PERK was found in 130 of 203 CRCs (64.04 %). P-PERK levels were negatively correlated with tumor stage ( $p = 0.003$ ), T ( $p < 0.001$ ), N ( $p = 0.01$ ), M ( $p = 0.021$ ), and tumor differentiation ( $p = 0.048$ , Table 1). Univariate analysis revealed

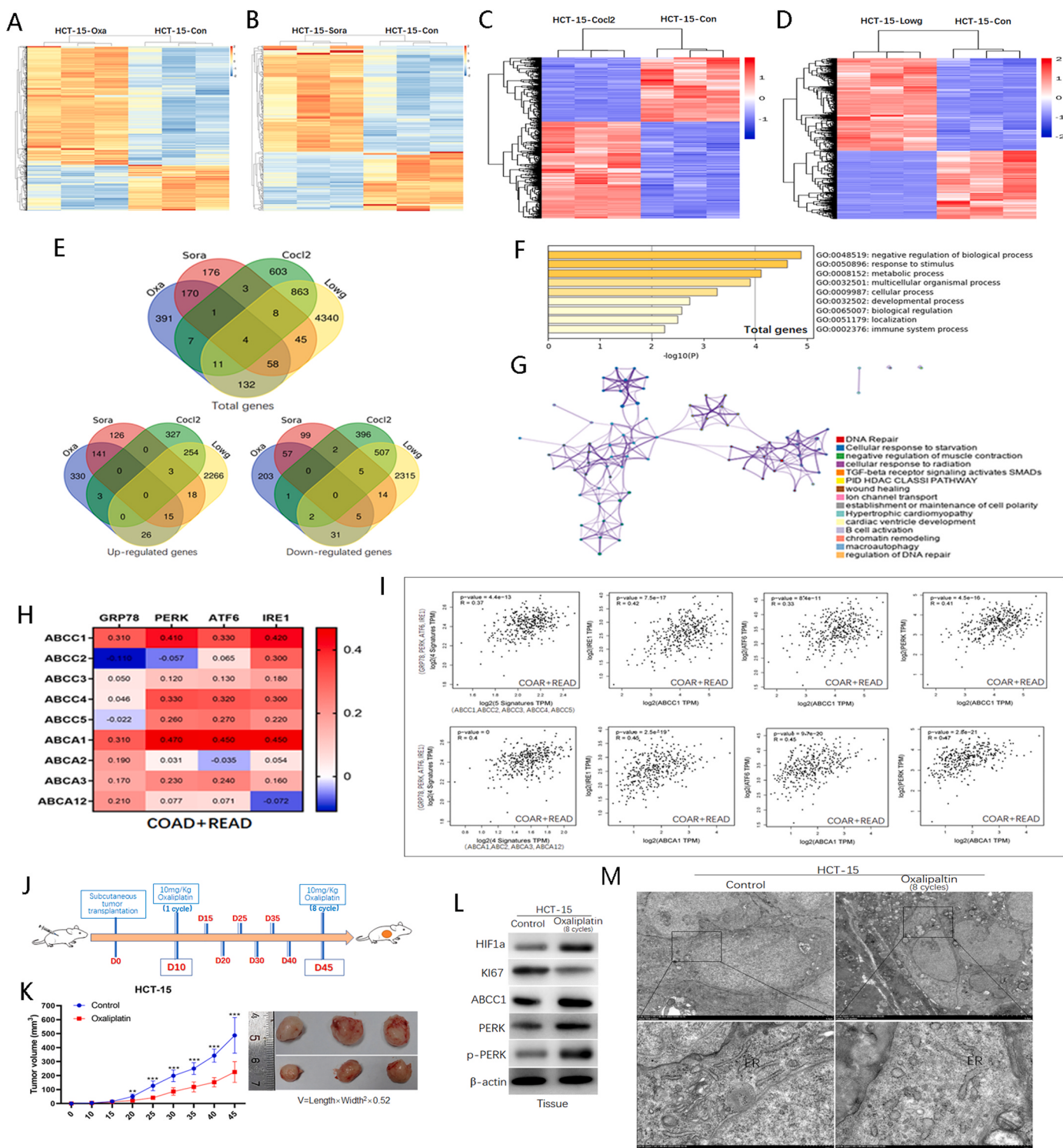


**Fig. 1.** CRC treated by four representative compounds exhibited oxaliplatin resistance with the mechanism of response to stimulus. RNA-Seq identified DEGs in four oxaliplatin-resistant CRC cell lines, HCT-15-Oxa (A), HCT-15-Sora (B), HCT-15-Cocl<sub>2</sub> (C), and HCT-15-Lowg (D), compared to the control cells. Total DEGs, upregulated DEGs, and downregulated DEGs from HCT-15-Oxa, HCT-15-Sora, HCT-15-Cocl<sub>2</sub>, and HCT-15-Lowg cells had multiple genes overlap (E). GO enrichment analysis for overlapping DEGs showed the enrichment in response to stimulus (F–G). TCGA database revealed the relationships between individual MRP subfamily genes and ER stress genes, and we demonstrated a positive correlation between MRP gene signatures and ER stress gene signatures in colon and rectal adenocarcinoma (H–I). Schematic diagram of the method used to generate oxaliplatin-resistant subcutaneous tumors (J). Oxaliplatin treatment resulted in smaller tumor volumes compared to the tumors of the control group mice (K). Sequential oxaliplatin therapy increased HIF1 $\alpha$ , ABCC1, PERK, and P-PERK levels in the residual tumors (L). TEM revealed the dilated, cystic ER structures in the oxaliplatin-treated tumor tissues (M).

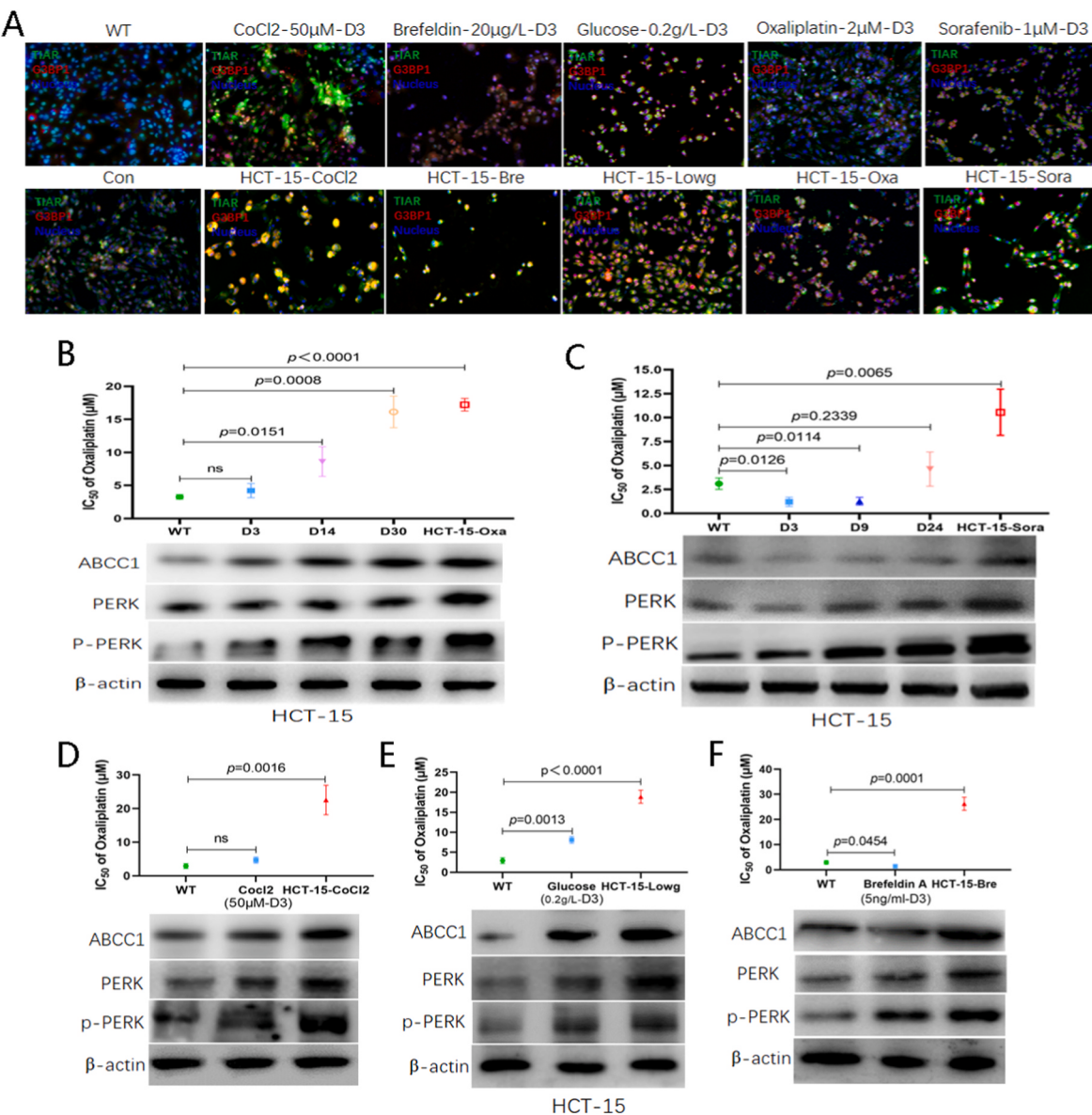


**Fig. 2.** Persistent external stimulus enhanced oxaliplatin resistance in CRC cells, whereas the resistance phenotype caused by short-term stimulus varied. Immunofluorescence showed the levels of stress granules, marked by TIAR and G3BP1 staining, in HCT-15 cells treated with different compounds for 3 days and for more than 30 days (A). During the course of oxaliplatin treatment, CRC cells gradually acquired oxaliplatin resistance and upregulated PERK, P-PERK, and ABCC1 levels (B). The correlations between the oxaliplatin IC<sub>50</sub> values and the PERK, P-PERK, and ABCC1 levels were inconsistent with continuous sorafenib treatment (C). The correlations between the oxaliplatin IC<sub>50</sub> values and the P-PERK and ABCC1 levels were inconsistent with continuous CoCl<sub>2</sub>, low glucose, or brefeldin A treatment, whereas the correlations were consistent when treatment continued longer than 30 days (D–F).

that sex (HR = 0.66, *p* = 0.023), tumor stage (HR = 6.474, *p* < 0.001), T (HR = 3.875, *p* = 0.001), N (HR = 5.526, *p* < 0.001), M (HR = 11.323, *p* < 0.001), vascular invasion (HR = 3.558, *p* < 0.001), and tumor differentiation (HR = 4.391, *p* < 0.001) were significantly associated with postoperative OS (Table 2). The multivariate Cox proportional hazards model revealed that sex (HR = 1.556, *p* = 0.018), T (HR = 2.34, *p* = 0.047), M (HR = 5.679, *p* < 0.001), and tumor differentiation (HR = 2.053, *p* = 0.04) were significantly associated with postoperative OS (Table 3). Moreover, Kaplan-Meier analysis demonstrated that patients in the P-PERK<sup>high</sup> group had a significantly longer 5-year OS (HR = 0.3234, *p* < 0.001) and a lower 5-year cumulative recurrence rate (HR = 0.3582, *p* < 0.001) than those in the P-PERK<sup>low</sup> group (Fig. 4E and F).

We also evaluated the role of P-PERK in CRC in vitro. HCT-15 cell proliferation was significantly inhibited by treatment with CCT020312, a PERK activator (*p* < 0.001, Fig. 4G). HCT-15 cells treated with CCT020312 were also more resistant to oxaliplatin (*p* = 0.0084;

Fig. 4H). Conversely, treatment of HCT-15 cells with the PERK inhibitor GSK2656157 resulted in significantly increased proliferation (Fig. 4I) and less oxaliplatin resistance (Fig. 4J). In addition, HCT-15 cells (5 × 10<sup>6</sup> cells) were subcutaneously injected into the right sides of the necks of 4-week-old male BALB/c nu mice (n = 5/group). After 5 weeks, subcutaneous tumor-bearing mice were euthanized, and the tumor weights were evaluated. Tumor growth was significantly inhibited by treatment with the PERK activator CCT020312 (*p* = 0.0012). When combined with oxaliplatin, the tumor weights did not decrease further (*p* > 0.05). Conversely, when treated with the PERK inhibitor GSK2656157, the tumor weights increased (*p* = 0.0019), and a synergistic antitumor effect with a significant decrease in tumor weight occurred when combined with oxaliplatin treatment (*p* < 0.05) (Fig. 4K). These findings established that PERK was a key regulator of malignant CRC progression relating senescence and translational elongation inhibition.

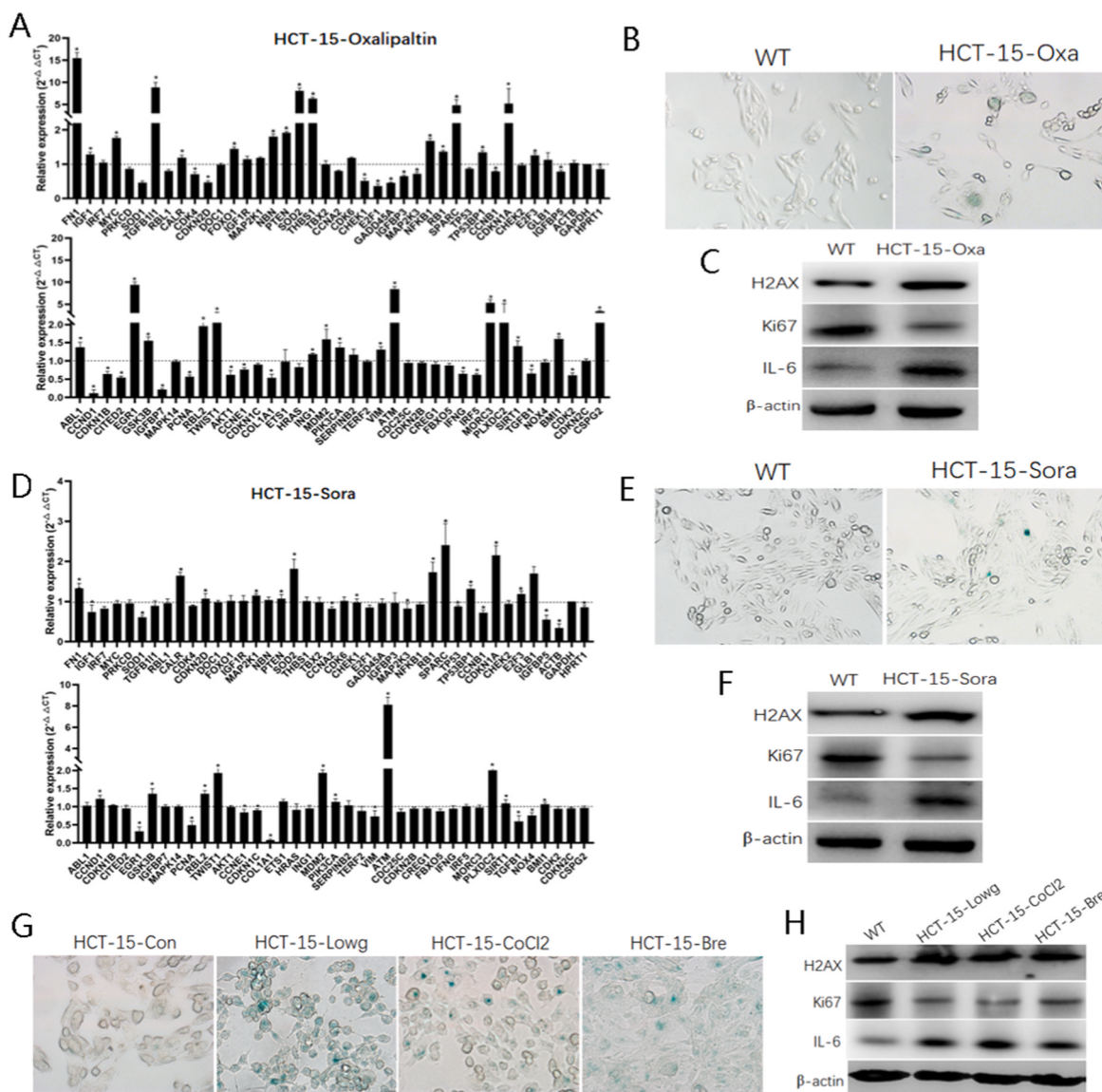


**Fig. 3.** Oxaliplatin-resistant CRC cells resulting from long-term stimulus induced senescence with diverse compounds  
PCR array revealed the senescence-associated genes in HCT-15-Oxa and HCT-15-Sora (A). SA- $\beta$ -gal staining showed the senescent cells in HCT-15 after long-term oxaliplatin treatment (B). Immunoblotting confirmed higher levels of senescence-related proteins (C). Similarly, PCR array and immunoblotting confirmed the upregulation of senescence-associated genes and proteins (D, F). SA- $\beta$ -gal staining also revealed an increased number of senescent cells after long-term sorafenib treatment (E). SA- $\beta$ -gal staining revealed an increased number of senescent cells after treatment with CoCl<sub>2</sub>, brefeldin A, or low glucose for more than 30 days (G), and immunoblotting confirmed increased levels of senescence-associated proteins (H).

### 3.5. IP6 had a strong affinity for ER stress sensors based on molecular docking and SPR analyses

Molecular docking is a structure-based computational algorithm for compound screening. Considering the roles of traditional Chinese medicine and natural compounds in antitumor research [27], we screened the Database of US Food and Drug Administration-approved antioxidants using the PyRx virtual screening tool AutoDock Vina. From this screen, we analyzed the binding energy (BE) values between ten of the common antioxidant compounds and GRP78, including maslinic acid (BE: -6.28), the proanthocyanidins (BE: -2.94), resveratrol (BE: -5.1), tanshinone IIA (BE: -7.71), vitamin E (BE: -4.73), glycyrrhizin (BE: -3.25), ammonium glycyrrhizinate (BE: -3.31), curcumin (BE: -5.45), glutathione (BE: -3.79), and IP6 (BE: -13.67) (Fig. 5A and B, Figs. S4–5). Because IP6 could achieve low-energy binding with GRP78, we further explored the BE values between IP6 and other ER stress sensors, including eEF2 (BE: -7.3), ATF6 (BE:

-6.02), IRE1 (BE: -7.11), PERK (BE: -7.24), and DPH1 (BE: -13.25) (Fig. 5C–D and Fig. S6). We also performed real-time SPR analysis and found strong affinities between IP6 and GRP78 ( $K_D = 4.407 \times 10^{-4}$ ) (Fig. 5E and F) and IP6 and DPH1 ( $K_D = 5.598 \times 10^{-5}$ ) (Fig. 5G and H), whereas the BE between IP6 and eEF2K was very high ( $K_D = 58.63$ ) (Fig. S8).

### 3.6. IP6 and oxaliplatin demonstrated significant synergistic antitumor efficacy against CRC

Based on the findings of this study and our previous study [28], we hypothesized that IP6 could have a direct anticancer effect or reverse CRC chemoresistance associated with the UPR. We observed that IP6 exhibited milder anticancer effects on the oxaliplatin-resistant HCT-15-Oxa cells ( $IC_{50} = 5.28 \mu M$ ) (Fig. 6A) and HT-29-Oxa ( $IC_{50} = 9.13 \mu M$ ) (Fig. 6C). The combination of IP6 and oxaliplatin synergistically decreased the oxaliplatin  $IC_{50}$  for the HCT-15-Oxa (Fig. 6B) and

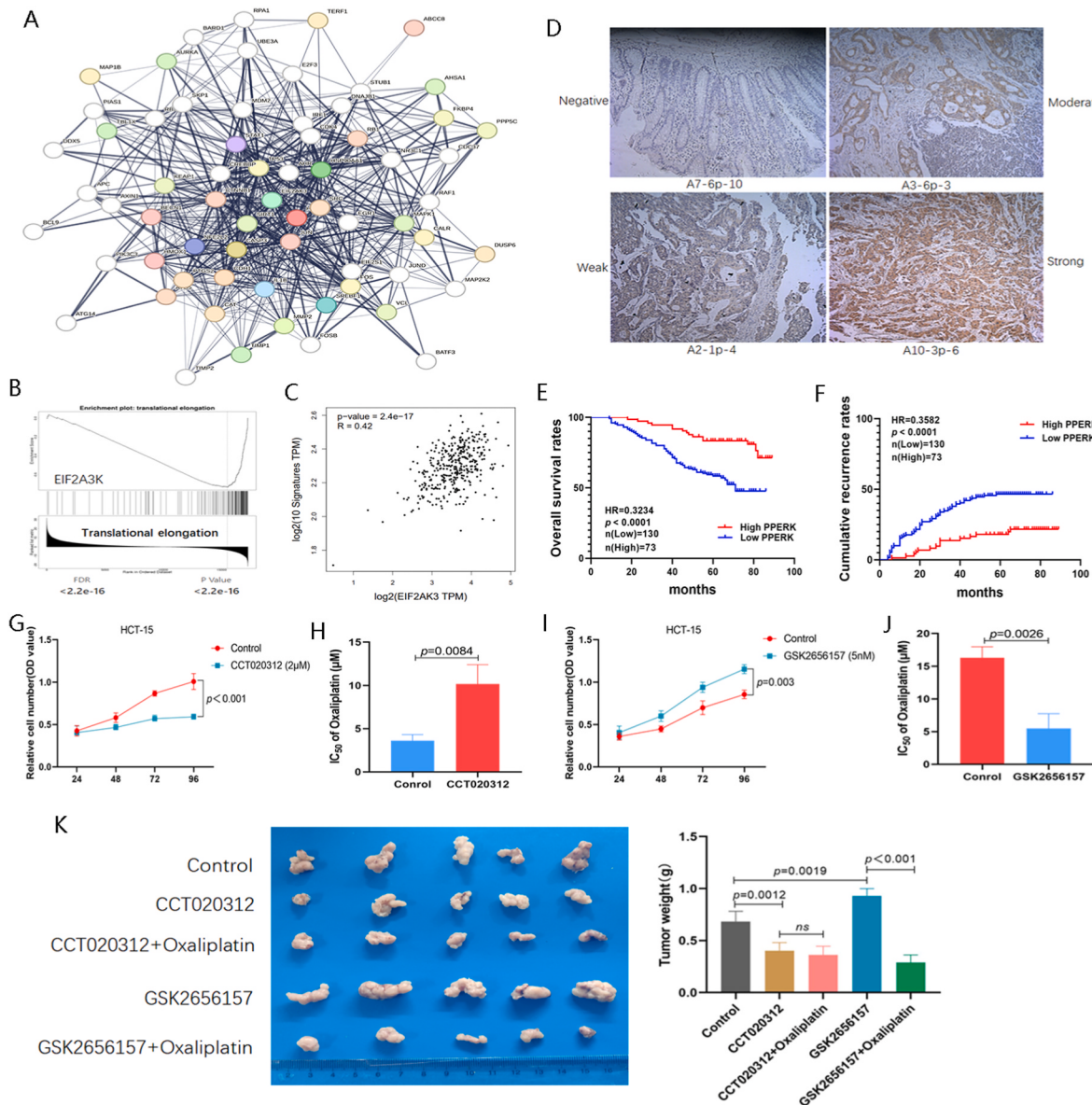


**Fig. 4.** PERK was acting as a key regulator of malignant CRC progression relating senescence and translational elongation inhibition. STRING analysis revealed that the ER sensors PERK/EIF2AK3 played a central role in the processes of ER stress, senescence, and chemoresistance (A). LinkedOmics analysis revealed that PERK was negatively related to translational elongation (B). GEPIA2 analysis revealed the correlation between PERK and senescence signatures (ten senescence-associated genes, C). Representative immunostaining images of different P-PERK levels in CRC patient tumors (D). Kaplan-Meier curves for OS (E) and CCR (F) rates according to P-PERK expression. High P-PERK levels were associated with poor prognosis in CRC. Treatment of HCT-15 cells with the PERK activator CCT020312 significantly inhibited proliferation (G) and enhanced oxaliplatin resistance (H). Treatment of HCT-15-Oxa cells with the PERK inhibitor GSK2656157 resulted in significantly increased proliferation (I) and increased oxaliplatin sensitivity (J). Combined antitumor assays were performed in vivo, and the roles of PERK activators and inhibitors exhibited the same trends when combined with oxaliplatin as demonstrated in vitro (K).

HT-29-Oxa (Fig. 6D) cells. Furthermore, the addition of IP6 to the oxaliplatin treatment increased the numbers of apoptotic HCT-15-Oxa ( $p = 0.001$ ; Fig. 6E) and HT-29-Oxa cells ( $p = 0.0031$ ; Fig. 6F).

In vivo, the combination of oxaliplatin and IP6 significantly decreased the volume of the subcutaneous xenografts in nude mice. The subcutaneous tumors in the combination treatment group were smaller than those from mice treated with oxaliplatin ( $p < 0.0001$ ) or IP6 ( $p < 0.0001$ ) alone, although both agents had significant anticancer effects by themselves ( $p = 0.0013$  and  $p = 0.0205$ , respectively) (Fig. 6G and H). We also examined the effects of oxaliplatin, IP6, and their combination on an abdominal CRC tumor model. Both oxaliplatin ( $p < 0.0001$ ) and IP6 ( $p < 0.0001$ ) alone had significant anticancer effects, as indicated by reduced tumor bioluminescence values (Fig. 6I and J). In addition, the combined treatment with oxaliplatin and IP6 prolonged

mouse survival compared to treatment with oxaliplatin alone ( $p = 0.0064$ ; Fig. 6K).

Using immunohistochemistry, we investigated the role of IP6 in modulating UPR and senescence in vivo. We observed decreased proportions of cells stained for ABCC1, P-PERK, ATM, and Ki67 in the tumor tissues from mice cotreated with IP6 and oxaliplatin compared to those treated with oxaliplatin alone. Compared to the control tumors, significant decreases in the ABCC1, P-PERK, and Ki67 levels were also observed after treatment with IP6 alone (Fig. 6L). Finally, TEM revealed that oxaliplatin and IP6 combination therapy restored the cord-like ER structure lost by treatment with oxaliplatin alone (Fig. 6M). Additionally, in vitro and in vivo experiments revealed that IP6 therapy in concentration and time gradients exhibited no significant acute toxicity (Fig. S9). These data demonstrated that IP6 could enhance the killing of

**Table 1**

Correlations between PPERK and clinicopathology feature in 203 patients with CRC.

Variable	No. Of Patient			Variable	No. Of Patient		
	PPERK <sup>high</sup>	PPERK <sup>low</sup>	P value		PPERK <sup>high</sup>	PPERK <sup>low</sup>	P value
Age, y	47	75	0.350	M	71	114	<b>0.021</b>
≥65	26	55		M0	2	16	
<65				M1			
Sex	30	56	0.784	Vascular invasion	2	12	0.080
Men	43	74		Yes	71	118	
Women				No			
Location	25	59	0.073	Tumor differentiation	67	106	<b>0.048</b>
Ascending colon	11	8		High	6	24	
Transverse colon	5	15		Low			
Descending colon	32	48					
Sigmoid & Rectum Colon							
Stage	48	57	<b>0.003</b>	Ki67	29	10	<0.001
I-II	25	73		Negative	44	120	
III-IV				Positive			
T	20	11	<0.001	KLF4	25	53	0.359
T1 - T2	53	119		Negative	48	77	
T3 - T4				Positive			
N	49	59	<b>0.010</b>	FoxM1	32	39	<b>0.047</b>
N0	14	47		Negative	41	91	
N1	10	24		Positive			
N2							

**Table 2**

Univariate analysis of factors associated with survival (n = 203).

Variables	Overall Survival		Disease Free Survival	
	Hazard ratio (95 % confidence interval)	P value	Hazard ratio (95 % confidence interval)	P value
Age, y, ≥65 vs < 65	0.951 (0.673–1.345)	0.778	0.994 (0.667–1.334)	0.544
Sex, male vs female	0.660 (0.461–0.944)	<b>0.023</b>	1.554 (1.087–2.222)	<b>0.016</b>
Stage, III-VI vs I-II	6.474 (3.770–11.118)	<b>0.001</b>	6.290 (3.666–10.790)	<b>0.001</b>
T, T3-T4 vs T1-T2	3.875 (1.707–8.794)	<b>0.001</b>	3.852 (1.638–8.742)	<b>0.001</b>
N, N1–N2 vs N0	5.526 (3.381–9.032)	<b>0.001</b>	5.184 (3.182–8.447)	<b>0.001</b>
M, M1 vs M0	11.323 (7.403–17.318)	<b>0.001</b>	9.818 (6.416–15.021)	<b>0.001</b>
Vascular invasion, yes vs no	3.558 (2.304–5.495)	<b>0.001</b>	3.528 (2.286–5.444)	<b>0.001</b>
Tumor differentiation, low vs high	4.391 (3.046–6.330)	<b>0.001</b>	4.047 (2.806–5.836)	<b>0.001</b>
PPERK, high vs low	0.323 (0.207–0.504)	<b>0.001</b>	0.365 (0.236–0.564)	<b>0.001</b>

chemoresistant CRC by modulating UPR during ER stress and improving senescence in vivo.

### 3.7. Diphthamide modification was required for eEF2-induced chemoresistance and IP6-mediated UPR and inhibited chemoresistance by decreasing the ADPr-eEF2 levels in CRC cells

Based on the low BE of IP6 with DPH1 and GRP78, we inferred that IP6 might directly affect the functions of UPR and the diphthamide modification of eEF2. First, we determined that the diphthamide modification of eEF2 was upregulated with increased ADPr-eEF2 levels during ER stress in HCT-15 treated with brefeldin A or thapsigargin (Fig. 7A). DPH1 knockdown in CRC cells downregulated ADPr-eEF2 levels; and this effect was abolished by DPH1 rescue (Fig. 7B). We next investigated whether DPH1 could bind to eEF2. Immunoprecipitation of exogenous Flag-tagged DPH1 and hemagglutinin-tagged eEF2 confirmed this interaction (Fig. 7C). The interaction between endogenous DPH1 and eEF2 was further confirmed by reciprocal co-

**Table 3**

Multivariate analysis of factors associated with survival (n = 203).

Variables	Overall Survival		Disease Free Survival	
	Hazard ratio (95 % confidence interval)	P value	Hazard ratio (95 % confidence interval)	P value
Sex, male vs female	1.556 (1.080–2.242)	<b>0.018</b>	1.695 (1.181–2.434)	<b>0.004</b>
Stage, III-VI vs I-II	1.625 (0.501–5.272)	0.419	2.174 (0.684–6.914)	0.188
T, T3-T4 vs T1-T2	2.340 (1.010–5.421)	<b>0.047</b>	2.449 (1.067–5.622)	<b>0.035</b>
N, N1–N2 vs N0	2.615 (0.888–7.705)	0.081	1.912 (0.671–5.448)	0.225
M, M1 vs M0	5.679 (3.375–9.557)	< 0.001	4.710 (2.807–7.901)	<b>0.001</b>
Vascular invasion, yes vs no	1.118 (0.684–1.828)	0.656	1.260 (0.776–2.047)	0.350
Tumor differentiation, low vs high	2.053 (1.257–3.353)	<b>0.004</b>	1.764 (1.073–2.900)	<b>0.025</b>
PPERK, high vs low	0.487 (0.308–0.771)	<b>0.002</b>	0.539 (0.344–0.845)	<b>0.007</b>

immunoprecipitation (Fig. 7D). In addition, we tested whether ER stress could increase the interaction between DPH1 and eEF2. Indeed, ER stress induced by brefeldin A significantly increased the interaction between these two proteins (Fig. 7E). We also examined the effect of the GRP78 inhibitor HA15 on the interaction between DPH1 and eEF2. Co-immunoprecipitation experiments revealed that the association between DPH1 and eEF2 in HCT-15 cells was enhanced by treatment with HA15 (Fig. 7F). Based on these results, we tested whether GRP78 could bind to DPH1 or eEF2 under normal physiological conditions and during ER stress. We observed that endogenous GRP78 bound to endogenous DPH1 under normal physiological conditions, whereas interaction between GRP78 and eEF2 was not detectable (Fig. 7G). Furthermore, the interaction between GRP78 and DPH1 in HCT15 cells was significantly inhibited by brefeldin A or HA15 (Fig. 7H). Considering that GRP78 sequesters inactive ER stress sensors in unstressed cells, our results indicate that competitive sequestration of DPH1 by GRP78 regulates the interaction between DPH1 and eEF2 and the diphthamide modification of eEF2.

Additionally, diphthamide modification of eEF2 needed to be

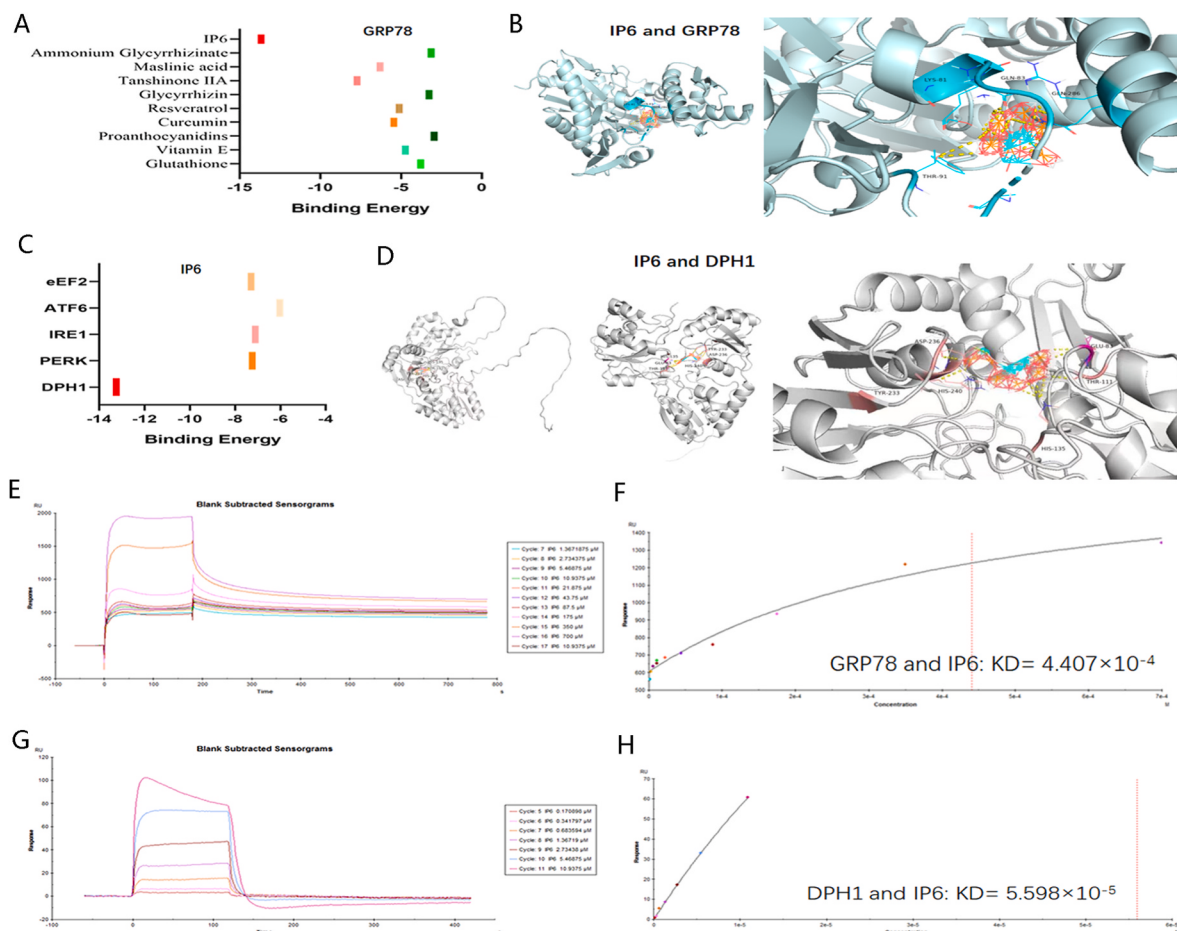


**Fig. 5.** IP6 had a strong affinity for ER stress sensors based on molecular docking and SPR analysis

Molecular docking analyzed the BE values between 10 common antioxidant compounds and GRP78 (A), and IP6 exhibited low-energy binding with GRP78 (B). Molecular docking analyzed the BE values between IP6 and other ER stress sensors (C), and IP6 exhibited low-energy binding with DPH1 (D). Real-time SPR revealed strong affinities between IP6 and GRP78 (E–F) and DPH1 (G–H).

verified in acquired chemoresistance. Diphthamide deficiency can be induced by deletion of the genes involved in diphthamide biosynthesis (DPH1–DPH7). However, these genes may have pleiotropic functions [29]. Therefore, we chose to introduce a point mutation by changing Gly<sup>717</sup> to Arg (eEF2<sup>G717R</sup>) in the eEF2 locus of CRC cells (Fig. 7I). Then, the downregulated ADPr-eEF2 levels in eEF2<sup>G717R</sup> mutant HCT-15 cells were verified by immunoblotting (Fig. 7J). We also verified the reduced protein affinity between eEF2 and DPH1 in eEF2<sup>G717R</sup> mutant cells by immunoprecipitation (Fig. 7K). In HCT-15-eEF2<sup>G717R</sup> and HT-29-eEF2<sup>G717R</sup> cells, oxaliplatin resistance was improved (Fig. 7L, and Fig. S11B), though after treatment with CCT020312, CRC cells with the eEF2<sup>G717R</sup> mutation exhibited no significant increase in ADPr-eEF2 levels and no enhanced resistance to oxaliplatin (Fig. 7L–M, and Figs. S11A–B). Furthermore, in oxaliplatin-resistant CRCs, the improvement of oxaliplatin resistance was more significant with the eEF2<sup>G717R</sup> mutant (Figs. S10A–B).

Based on the results of the molecular docking of IP6 with GRP78 and DPH1, we hypothesized that IP6 might directly affect the binding between GRP78 and DPH1 or PERK. Oxaliplatin-resistant CRC cells under ER stress were treated with IP6, and co-immunoprecipitation experiments revealed that IP6 altered the binding between GRP78 and PERK and decreased PERK phosphorylation (Fig. 7N). In addition, IP6 inhibited the ADPr of eEF2 (Fig. 7O) due to increased binding between GRP78 and DPH1 (Fig. 7P) and decreased the binding between DPH1 and eEF2 (Fig. 7Q and Fig. S10C). These results demonstrated that IP6 decreased ADPr-eEF2 and P-PERK levels by orchestrating the interaction among GRP78, DPH1, and eEF2, which orchestrated the UPR in

oxaliplatin-resistant CRC cells (Fig. 7R).

#### 4. Discussion

Oxaliplatin is an important chemotherapy agent that has benefited patients with advanced CRC by forming bulky DNA adducts and inducing apoptosis [30]. Frustratingly, randomized trials have shown fairly low efficacy of oxaliplatin monotherapy in CRC patients, and combined therapy with 5-fluorouracil and leucovorin is needed [31]. One reason for the unsatisfactory outcomes of oxaliplatin-based chemotherapy is acquired resistance. Thus, effective strategies for enhancing chemosensitivity are urgently needed [32]. In this study, we generated in vitro and in vivo CRC models that mimic the long-term oxaliplatin treatment of CRC patients. Using these models, we discovered that oxaliplatin resistance correlated with senescence and ER stress in CRC cells. However, the exact regulatory mechanisms linking chemoresistance, senescence, and ER stress are still vague and need further study [33].

Multiple stressors enriched in the tumor microenvironment dynamically perturb the protein-folding capacity of the ER in malignant tumors, and oncogenic signaling and the UPR in cancer cells sustain ER stress homeostasis in tumors [12]. Salaroglio et al. [34] demonstrated that activating the PERK/Nrf 2/MRP1 axis results in an oxaliplatin resistance phenotype in multiple tumors. This study confirmed the correlation between PERK phosphorylation and acquired chemoresistance in CRC induced by oxaliplatin, CoCl<sub>2</sub>, and low glucose. Paradoxically, sorafenib and brefeldin A also activated UPR in CRC

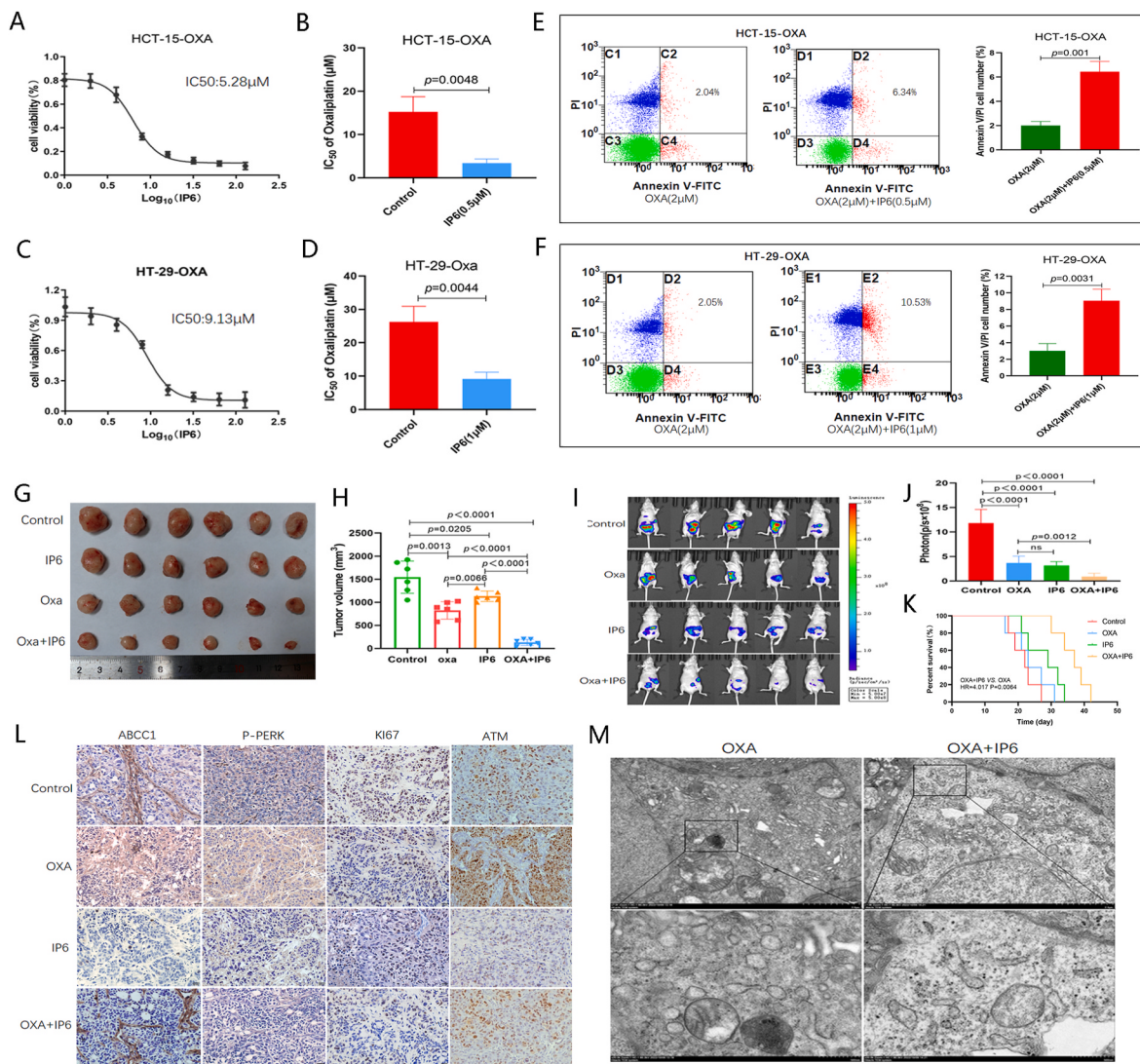


**Fig. 6.** IP6 and oxaliplatin demonstrated significant synergistic antitumor efficacy against CRC

IP6 exhibited milder anticancer effects on the oxaliplatin-resistant HCT-15-Oxa cells (A) and HT-29-Oxa cells (C). The combination of IP6 and oxaliplatin synergistically decreased the oxaliplatin IC<sub>50</sub> values in the HCT-15-Oxa cells (B) and HT-29-Oxa cells (D). The addition of IP6 to the oxaliplatin treatment increased the numbers of apoptotic HCT-15-Oxa cells (E) and HT-29-Oxa cells (F). Subcutaneous tumors in the combination treatment group were smaller than those from mice treated with oxaliplatin or IP6 alone (G–H). The combination of oxaliplatin and IP6 on an abdominal CRC tumor model also exhibited significant anticancer effects and prolonged mouse survival (J–K). Immunohistochemistry revealed the role of IP6 in modulating the UPR and senescence (L). TEM revealed that IP6 combination therapy restored the cord-like ER structure (M).

cells with a concomitant increase in PERK phosphorylation. Short-term stimulus with sorafenib or brefeldin A decreased oxaliplatin resistance and the expression of ABCC1; however, long-term stimulus of CRC cells with these agents enhanced oxaliplatin resistance. Sorafenib is a multikinase inhibitor capable of facilitating apoptosis and suppressing tumor cell proliferation through inhibiting the Ras/Raf/MEK/ERK/MAPK pathway, which are the upstream signaling mediators of ABCC1. Unfortunately, sorafenib resistance can develop upon the continuation of sorafenib treatment [35], and the upregulation of ABCC1 expression contributes to sorafenib resistance [36]. It was previously demonstrated that increased levels of ABCC1 are involved in cellular defense mechanisms, especially multidrug resistance [37]. Similarly, brefeldin A, an inhibitor of protein transport from the ER to the Golgi apparatus, inhibits cell growth, migration, and drug resistance related to the MAPK and AKT signaling pathways [38,39]. After long-term treatment with brefeldin A, our data revealed increases in PERK phosphorylation and ABCC1 expression. In this study, our data also demonstrated that long-term stimulus was correlated with CRC cell

senescence. Cellular senescence used to be considered an essential tumor suppressive mechanism that prevents the propagation of oncogenically activated and genetically unstable cells [40]. However, an increasing body of evidence has shown that radiation and chemotherapy cause the accumulation of senescent cells in tumors that, paradoxically, promote tumor relapse, metastasis, and chemoresistance [41]. Therefore, therapy-induced ER stress and the associated senescence would be a potential target for improving anticancer therapy.

Based on the literature and our findings, ER stress, senescence, and oxaliplatin resistance are closely correlated. Thus, it was crucial to identify the core mediator linking these three processes [7,42]. Using STRING and GEPIA2, we identified the ER stress sensor PERK as such a key mediator. The clinical role of P-PERK was established using a cohort of CRC patients. It has been reported that inhibition of PERK can interfere with the assembly of respiratory supercomplexes, whereas PERK activation is sufficient to increase supercomplex formation and promote mitochondrial respiration under glucose-free conditions [43]. In this study, we found that treatment of oxaliplatin-resistant CRC cells

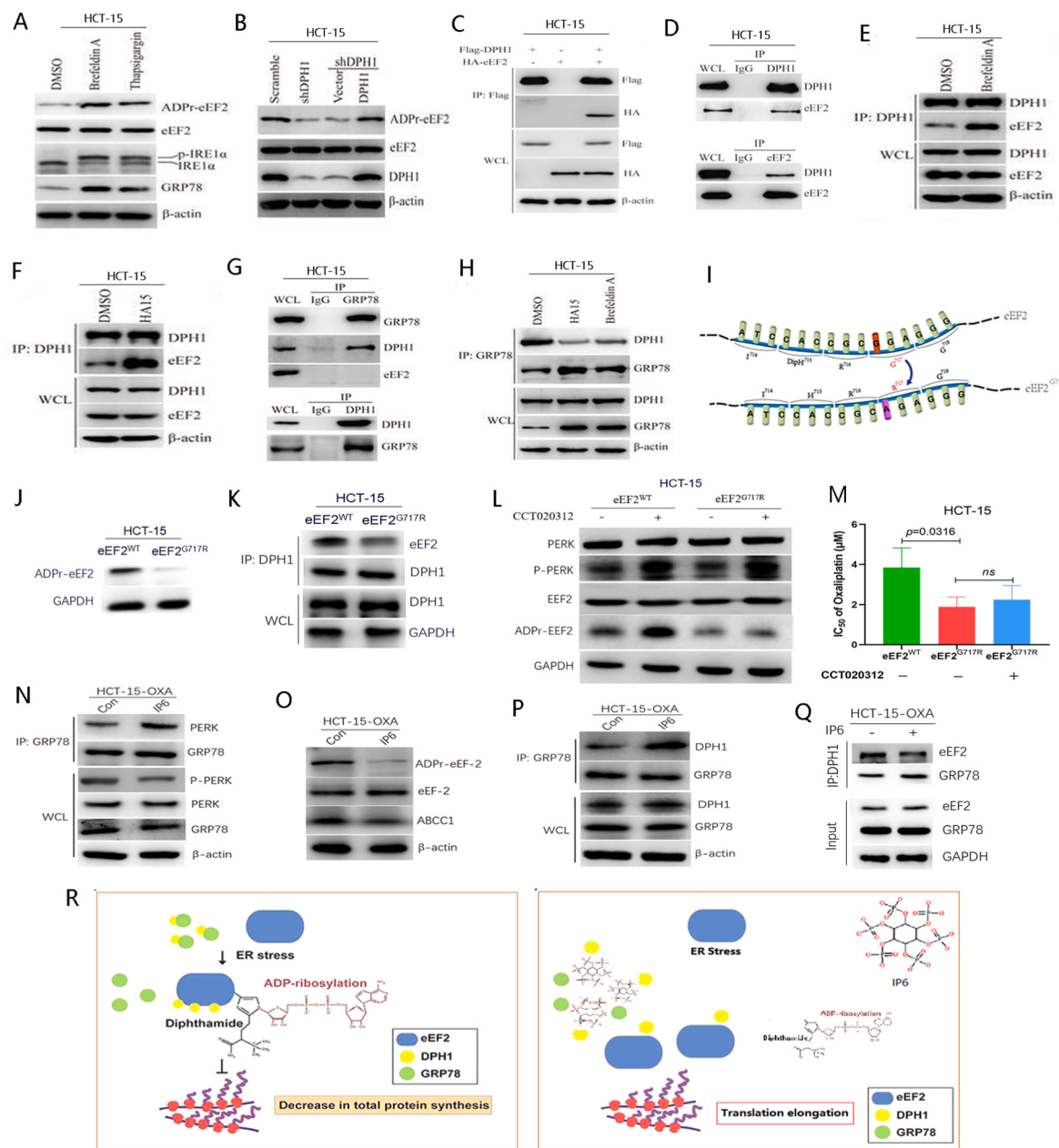


**Fig. 7.** IP6 orchestrated UPR by decreasing P-PERK and ADPr-eEF-2 levels in CRC cells

Brefeldin A and thapsigargin increased ADPr-eEF2 levels in HCT-15 cells under ER stress (A). ADPr-eEF2 levels were downregulated in DPH1 knockdown CRC cells. ADPr levels on eEF2 were restored after DPH1 rescue (B). The interaction between exogenous DPH1 and eEF2 was confirmed by co-immunoprecipitation (C). The interaction between endogenous DPH1 and eEF2 was reciprocally demonstrated by co-immunoprecipitation (D). Brefeldin A increased the interaction between DPH1 and eEF2 in cells under ER stress (E). Co-immunoprecipitation revealed that the association between DPH1 and eEF2 was enhanced in HCT-15 cells after treatment with GRP78 inhibitor HA15 (F). Co-immunoprecipitation showed that endogenous GRP78 binds to endogenous DPH1 under physiological conditions; however, the interaction between GRP78 and eEF2 was not detectable (G). The interaction between GRP78 and DPH1 was significantly inhibited in HCT15 cells treated with brefeldin A or HA15 (H). A point mutation changing Gly<sup>717</sup> to Arg (eEF2<sup>G717R</sup>) in the eEF2 locus was performed in CRC cells (I). The downregulation of ADPr-eEF2 levels in eEF2<sup>G717R</sup> mutant HCT-15 cells was demonstrated by immunoblotting (J). Reduced protein affinity between eEF2 and DPH1 was demonstrated in eEF2<sup>G717R</sup> mutant cells by immunoprecipitation (K). HCT-15-eEF2<sup>G717R</sup> cells treated with CCT020312 exhibited no significant increase in ADPr-eEF2 levels (L) and no enhanced resistance to oxaliplatin (M). Co-immunoprecipitation showed that IP6 weakened the binding between GRP78 and PERK, decreasing P-PERK levels (N). IP6 inhibited the expression of ADPr-eEF2 (O) by increasing the binding between GRP78 and DPH1 (P). A Co-IP pull-down assay with DPH1 revealed that IP6 decreased the binding between DPH1 and eEF2 (Q). Schematic diagram illustrated that IP6 decreased ADPr-eEF2 and P-PERK levels by orchestrating the interaction between GRP78 and DPH1 or PERK (R).

with a PERK inhibitor partially restored proliferation and decreased oxaliplatin resistance and the number of senescent cells. Activation of the PERK pathway reduces the protein load on the ER by retarding translational elongation, restoring normal ER function [44]. This process allows cells to adapt to oxaliplatin treatment.

Traditional Chinese medicine has been used to treat malignant

tumors for thousands of years in China, exhibiting outstanding anti-cancer effects and minimal side effects [45]. Many natural antioxidants in Chinese herbals have been used to prevent and treat cancer, including curcumin, resveratrol, and tanshinone IIA [46]. Several studies have found that natural plant-based bioactive compounds can enhance the efficacy of chemotherapy; however, several have failed in the treatment

of cancer [47]. Therefore, it is important to identify effective natural compounds and potential mechanisms based on persistent ER stress induced by oxaliplatin. Using molecular docking and SPR analysis, we discovered that GRP78 and DPH1 had strong BE with IP6, a naturally occurring, non-toxic product. IP6 treatment decreased ADPr-eEF-2 and P-PERK levels, resulting in the enhanced killing of chemoresistant CRC through the modulation of UPR in vivo. IP6 is abundant in grains and acts as a broad-spectrum antineoplastic agent. Its molecular structure, which features multi-phosphate groups surrounding a central inositol ring, is a highly reactive ligand that can interact with various cations, small molecules, and polymers [48]. Our previous study showed that IP6 acts synergistically with oxaliplatin to reduce the proliferation of hepatocellular carcinoma through the downregulation of the CCN2-LRP6-β-catenin-ABCG1 signaling pathway [28]. Fu et al. demonstrated that IP6 could reduce the migration and invasiveness of colorectal cancer cells and prevent their metastasis to the liver [49]. Wang et al. determined that IP6 reacted with cisplatin to form uniform nanoparticles with enhanced anticancer effects [50]. In the present study, we showed that IP6 enhanced the killing of chemoresistant CRC cells by modulating UPR induced by ER stress, which may represent a new combined intervention strategy for improving CRC chemoresistance.

## Funding

This study was sponsored by grants from the Natural Science Foundation of Shandong Province (ZR2020MH253), the Natural Science Basic Research Program of Shaanxi Province (2022JQ-832), the National Natural Science Foundation of China (82,203,047), and the Open Funds for Shaanxi Provincial Key Laboratory of Infection and Immune Diseases (2022-KFZD-1).

## CRediT authorship contribution statement

**Binghui Xu:** Writing – review & editing, Writing – original draft, Methodology, Investigation, Data curation. **Qingan Jia:** Writing – review & editing, Writing – original draft, Supervision, Methodology, Investigation, Funding acquisition, Data curation, Conceptualization. **Xia Liao:** Visualization, Methodology, Investigation, Funding acquisition, Data curation. **Tian Fan:** Methodology, Data curation. **Lei Mou:** Data curation. **Yuna Song:** Data curation. **Chunyu Zhu:** Visualization. **Tongling Yang:** Data curation. **Zhixian Li:** Supervision. **Miao Wang:** Supervision. **Qiangbo Zhang:** Writing – review & editing, Writing – original draft, Supervision, Resources, Investigation, Funding acquisition, Conceptualization. **Lei Liang:** Writing – original draft, Supervision, Project administration, Conceptualization.

## Declaration of competing interest

The authors declare that they have no known competing financial interests or personal relationships that could have appeared to influence the work reported in this paper.

## Acknowledgements

Not applicable.

## List of abbreviations

CRC	colorectal cancer
ER	endoplasmic reticulum
GRP78	glucose-regulating protein 78
IRE1α	inositol-requiring enzyme 1α
ATF6	activating transcription factor 6
PERK	protein kinase R-like ER kinase
P-PERK	phosphorylated PERK

UPR	unfolded protein response
mRNA	messenger RNA
eEF-2	eukaryotic translation elongation factor 2
ADPr	adenosine diphosphate-ribosylation
eIF2α	translation initiation factor2-α
IP6	inositol hexaphosphate
DPH1	diphthamide biosynthesis gene 1
SPR	surface plasmon resonance
IgG	immunoglobulin G
RNA-Seq	RNA sequencing
cDNA	complementary DNA
KEGG	Kyoto Encyclopedia of Genes and Genomes
DEGs	differentially expressed genes
GO	Gene Ontology
TCGA	The Cancer Genome Atlas
MRPs	multidrug resistance proteins
TEM	transmission electron microscopy
HIF1α	hypoxia-inducible factor-1α

## Appendix A. Supplementary data

Supplementary data to this article can be found online at <https://doi.org/10.1016/j.canlet.2023.216591>.

## References

- [1] H. Sung, J. Ferlay, R.L. Siegel, M. Laversanne, I. Soerjomataram, A. Jemal, F. Bray, Global cancer statistics 2020: GLOBOCAN estimates of incidence and mortality worldwide for 36 cancers in 185 countries, CA A Cancer J. Clin. 71 (2021) 209–249.
- [2] F. Di Nicolantonio, P.P. Vitiello, S. Marzoni, S. Siena, J. Tabernero, L. Trusolino, R. Bernards, A. Bardelli, Precision oncology in metastatic colorectal cancer - from biology to medicine, Nat. Rev. Clin. Oncol. 18 (2021) 506–525.
- [3] R. Gosavi, C. Chia, M. Michael, A.G. Heriot, S.K. Warrier, J.C. Kong, Neoadjuvant chemotherapy in locally advanced colon cancer: a systematic review and meta-analysis, Int. J. Colorectal Dis. 36 (2021) 2063–2070.
- [4] G. Bregni, T. Akin Telli, S. Camera, A. Deleporte, L. Moretti, A.M. Bali, G. Liberale, S. Holbrechts, A. Hendliz, F. Sclafani, Adjuvant chemotherapy for rectal cancer: current evidence and recommendations for clinical practice, Cancer Treat. Rev. 83 (2020), 101948.
- [5] Y.J. Chern, I.T. Tai, Adaptive response of resistant cancer cells to chemotherapy, Cancer Biol. Med. 17 (2020) 842–863.
- [6] M. Wang, R.J. Kaufman, Protein misfolding in the endoplasmic reticulum as a conduit to human disease, Nature 529 (2016) 326–335.
- [7] H.M. Ashraf, J. Moser, S.L. Spencer, Senescence evasion in chemotherapy: a sweet spot for p21, Cell 178 (2019) 267–269.
- [8] A. Kowald, J.F. Passos, T.B.L. Kirkwood, On the evolution of cellular senescence, Aging Cell 19 (2020), e13270.
- [9] C. Hetz, F.R. Papa, The unfolded protein response and cell fate control, Mol. Cell 69 (2018) 169–181.
- [10] E. Madden, S.E. Logue, S.J. Healy, S. Manie, A. Samali, The role of the unfolded protein response in cancer progression: from oncogenesis to chemoresistance, Biol. Cell. 111 (2019) 1–17.
- [11] R.L. Wiseman, J.S. Mesgarzadeh, L.M. Hendershot, Reshaping endoplasmic reticulum quality control through the unfolded protein response, Mol. Cell 82 (2022) 1477–1491.
- [12] X. Chen, J.R. Cubillos-Ruiz, Endoplasmic reticulum stress signals in the tumour and its microenvironment, Nat. Rev. Cancer 21 (2021) 71–88.
- [13] M. Bektaş, H. Akçakaya, A. Aroymak, R. Nurten, E. Bermek, Effect of oxidative stress on in vivo ADP-ribosylation of eukaryotic elongation factor 2, Int. J. Biochem. Cell Biol. 37 (2005) 91–99.
- [14] M. Costa-Mattioli, P. Walter, The integrated stress response: from mechanism to disease, Science 368 (2020).
- [15] S.J. Marciniak, J.E. Chambers, D. Ron, Pharmacological targeting of endoplasmic reticulum stress in disease, Nat. Rev. Drug Discov. 21 (2022) 115–140.
- [16] E. Bahar, J.Y. Kim, H. Yoon, Chemotherapy resistance explained through endoplasmic reticulum stress-dependent signaling, Cancers (2019) 11.
- [17] Q.A. Jia, Z.G. Ren, Y. Bu, Z.M. Wang, Q.B. Zhang, L. Liang, X.M. Jiang, Q.B. Zhang, Z.Y. Tang, Herbal compound "songyou yin" renders hepatocellular carcinoma sensitive to oxaliplatin through inhibition of stemness, Evid Based Complement Alternat Med. (2012), 908601, 2012.
- [18] S.H. Liu, C. Bachran, P. Gupta, S. Miller-Randolph, H.L. Wang, D. Crown, Y. Zhang, A.N. Wein, R. Singh, R. Fattah, S.H. Leppla, Diphthamide modification on eukaryotic elongation factor 2 is needed to assure fidelity of mRNA translation and mouse development, P Natl Acad Sci USA 109 (2012) 13817–13822.
- [19] S. Dallakyan, A.J. Olson, Small-molecule library screening by docking with PyRx, Methods Mol. Biol. 1263 (2015) 243–250.

- [20] Y. Shao, Z. Gao, P.A. Marks, X. Jiang, Apoptotic and autophagic cell death induced by histone deacetylase inhibitors, *Proc. Natl. Acad. Sci. U. S. A.* 101 (2004) 18030–18035.
- [21] Z. Tang, B. Kang, C. Li, T. Chen, Z. Zhang, GEPIA2: an enhanced web server for large-scale expression profiling and interactive analysis, *Nucleic Acids Res.* 47 (2019) W556–W560.
- [22] D. Szklarczyk, A.L. Gable, K.C. Nastou, D. Lyon, R. Kirsch, S. Pyysalo, N. T. Doncheva, M. Legeay, T. Fang, P. Bork, L.J. Jensen, C. von Mering, The STRING database in 2021: customizable protein-protein networks, and functional characterization of user-uploaded gene/measurement sets, *Nucleic Acids Res.* 49 (2021) D605–D612.
- [23] A. Cersek, C.S.D. Roxburgh, P. Strombom, J.J. Smith, L.K.F. Temple, G.M. Nash, J. G. Guillemin, P.B. Paty, R. Yaeger, Z.K. Stadler, K. Seier, M. Gonen, N.H. Segal, D. L. Reidy, A. Varghese, J. Shia, E. Vakiani, A.J. Wu, C.H. Crane, M.J. Gollub, J. Garcia-Aguilar, L.B. Saltz, M.R. Weiser, Adoption of total neoadjuvant therapy for locally advanced rectal cancer, *JAMA Oncol.* 4 (2018), e180071.
- [24] Y. Wang, Z. Zhao, F. Wei, Z. Luo, Y. Duan, Combining autophagy-inducing peptides and brefeldin A delivered by perinuclear-localized mesoporous silica nanoparticles: a manipulation strategy for ER-phagy, *Nanoscale* 10 (2018) 8796–8805.
- [25] R. Roskoski Jr., Targeting oncogenic Raf protein-serine/threonine kinases in human cancers, *Pharmacol. Res.* 135 (2018) 239–258.
- [26] J.W. Brewer, J.A. Diehl, PERK mediates cell-cycle exit during the mammalian unfolded protein response, *Proc. Natl. Acad. Sci. U. S. A.* 97 (2000) 12625–12630.
- [27] R. Lagoa, J. Silva, J.R. Rodrigues, A. Bishayee, Advances in phytochemical delivery systems for improved anticancer activity, *Biotechnol. Adv.* 38 (2020), 107382.
- [28] X. Liao, Y. Zhang, B. Xu, A. Ali, X. Liu, Q. Jia, Inositol hexaphosphate sensitizes hepatocellular carcinoma to oxaliplatin relating inhibition of CCN2-LRP6-beta-catenin-ABCG1 signaling pathway, *J. Cancer* 12 (2021) 6071–6080.
- [29] S. Stahl, A.R. da Silva Mateus Seidl, A. Ducret, S. Kux van Geijtenbeek, S. Michel, T. Racek, F. Birzele, A.K. Haas, R. Rueger, M. Gerg, G. Niederfellner, I. Pastan, U. Brinkmann, Loss of diphthamide pre-activates NF-kappaB and death receptor pathways and renders MCF7 cells hypersensitive to tumor necrosis factor, *Proc. Natl. Acad. Sci. U. S. A.* 112 (2015) 10732–10737.
- [30] A. Stein, D. Arnold, Oxaliplatin: a review of approved uses, *Expert Opin. Pharmacother.* 13 (2012) 125–137.
- [31] A. Lamarca, D.H. Palmer, H.S. Wasan, P.J. Ross, Y.T. Ma, A. Arora, S. Falk, R. Gillmore, J. Wadsley, K. Patel, A. Anthony, A. Maraveyas, T. Iveson, J. S. Waters, C. Hobbs, S. Barber, W.D. Ryder, J. Ramage, L.M. Davies, J. A. Bridgewater, J.W. Valle, G. Advanced Biliary Cancer Working, Second-line FOLFOX chemotherapy versus active symptom control for advanced biliary tract cancer (ABC-06): a phase 3, open-label, randomised, controlled trial, *Lancet Oncol.* 22 (2021) 690–701.
- [32] T.P. Reddy, U. Khan, E.A. Burns, M. Abdelrahim, Chemotherapy rechallenge in metastatic colon cancer: a case report and literature review, *World J. Clin. Oncol.* 11 (2020) 959–967.
- [33] Y.J. Chern, I.T. Tai, Adaptive response of resistant cancer cells to chemotherapy, *Cancer Biology & Medicine* 17 (2020) 842–863.
- [34] I.C. Salaroglio, E. Panada, E. Moiso, I. Buondonno, P. Provero, M. Rubinstein, J. Kopecka, C. Riganti, PERK Induces Resistance to Cell Death Elicited by Endoplasmic Reticulum Stress and Chemotherapy, vol. 16, *Molecular Cancer*, 2017.
- [35] W. Tang, Z. Chen, W. Zhang, Y. Cheng, B. Zhang, F. Wu, Q. Wang, S. Wang, D. Rong, F.P. Reiter, E.N. De Toni, X. Wang, The mechanisms of sorafenib resistance in hepatocellular carcinoma: theoretical basis and therapeutic aspects, *Signal Transduct. Targeted Ther.* 5 (2020) 87.
- [36] Y.S. Chang, C.W. Su, S.C. Chen, Y.Y. Chen, Y.J. Liang, J.C. Wu, Upregulation of USP22 and ABCC1 during sorafenib treatment of hepatocellular carcinoma contribute to development of resistance, *Cells* (2022) 11.
- [37] S. Nath, K. Daneshvar, N. Puri, P. Mukherjee, Chemosensitivity in Pancreatic Cancer Is Conferred by MUC1 Cytoplasmic Tail Binding to the Promoter Region of the ABCC1 (MRP-1) Gene, *Cancer Res.* 2012, p. 72.
- [38] R. Gupta, P. Malvi, K.R. Parajuli, R. Janostík, S. Bugide, G. Cai, L.J. Zhu, M. R. Green, N. Wajapeyee, KLF7 promotes pancreatic cancer growth and metastasis by up-regulating ISG expression and maintaining Golgi complex integrity, *Proc. Natl. Acad. Sci. U. S. A.* 117 (2020) 12341–12351.
- [39] Z. Zhang, L. Zhou, N. Xie, E.C. Nice, T. Zhang, Y. Cui, C. Huang, Overcoming cancer therapeutic bottleneck by drug repurposing, *Signal Transduct. Targeted Ther.* 5 (2020) 113.
- [40] P.G. Prasanna, D.E. Citrin, J. Hildesheim, M.M. Ahmed, S. Venkatachalam, G. Riscuta, D. Xi, G. Zheng, J.V. Deursen, J. Goronyi, S.J. Kron, M.S. Anscher, N. E. Sharpless, J. Campisi, S.L. Brown, L.J. Niedernhofer, A. O'Loghlen, A. G. Georgakilas, F. Paris, D. Gius, D.A. Gewirtz, C.A. Schmitt, M.E. Abazeed, J. L. Kirkland, A. Richmond, P.B. Romesser, S.W. Lowe, J. Gil, M.S. Mendonca, S. Burma, D. Zhou, C.N. Coleman, Therapy-induced senescence: opportunities to improve anticancer therapy, *J. Natl. Cancer Inst.* 113 (2021) 1285–1298.
- [41] T. Saleh, L. Tyutyunyk-Massey, D.A. Gewirtz, Tumor cell escape from therapy-induced senescence as a model of disease recurrence after dormancy, *Cancer Res.* 79 (2019) 1044–1046.
- [42] M. Milanovic, D.N.Y. Fan, D. Belenki, J.H.M. Dabritz, Z. Zhao, Y. Yu, J.R. Dorr, L. Dimitrova, D. Lenze, I.A. Monteiro Barbosa, M.A. Mendoza-Parra, T. Kanashova, M. Metzner, K. Pardon, M. Reimann, A. Trumpp, B. Dorken, J. Zuber, H. Gronemeyer, M. Hummel, G. Dittmar, S. Lee, C.A. Schmitt, Senescence-associated reprogramming promotes cancer stemness, *Nature* 553 (2018) 96–100.
- [43] P. Strzyz, ER stress boosts respiration, *Nat. Rev. Mol. Cell Biol.* 20 (2019) 453.
- [44] P. Walter, D. Ron, The unfolded protein response: from stress pathway to homeostatic regulation, *Science* 334 (2011) 1081–1086.
- [45] X. Liao, Y. Bu, Q.G. Jia, Traditional Chinese medicine as supportive care for the management of liver cancer: past, present, and future, *Genes Dis* 7 (2020) 370–379.
- [46] F.S. Li, J.K. Weng, Demystifying traditional herbal medicine with modern approach, *Nat. Plants* 3 (2017), 17109.
- [47] S. Subramaniam, K.R. Selvaduray, A.K. Radhakrishnan, Bioactive compounds: natural defense against cancer? *Biomolecules* (2019) 9.
- [48] R. Wang, S. Guo, Phytic acid and its interactions: contributions to protein functionality, food processing, and safety, *Compr. Rev. Food Sci. Food Saf.* 20 (2021) 2081–2105.
- [49] M. Fu, Y. Song, Z. Wen, X. Lu, L. Cui, Inositol hexaphosphate and inositol inhibit colorectal cancer metastasis to the liver in BALB/c mice, *Nutrients* 8 (2016).
- [50] C. Wang, L. Li, S. Zhang, Y. Yan, Q. Huang, X. Cai, J. Xiao, Y. Cheng, Carrier-free platinum nanomedicine for targeted cancer therapy, *Small* 16 (2020), e2004829.